

Quantifying Trapped Magnetic Vortex Losses in Niobium Resonators at mK Temperatures

D. Bafia,^{1,*} B. Abdisararov,^{1,2} R. Pilipenko,¹ Y. Lu,¹ G. Ereemeev,¹ A. Romanenko,¹ and A. Grassellino¹

¹*Fermi National Accelerator Laboratory, Batavia, Illinois 60510, USA*

²*Department of Electrical and Computer Engineering,
Old Dominion University, Norfolk, Virginia 23529, USA*

(Dated: March 24, 2025)

Trapped magnetic vortices in niobium can introduce microwave losses in superconducting devices, affecting both niobium-based qubits and resonators. While our group has extensively studied this problem at temperatures above 1 K, in this study we quantify for the first time the losses driven by magnetic vortices for niobium-based quantum devices operating down to millikelvin temperature, and in the low photon counts regime. By cooling a single interface system a 3-D niobium superconducting cavity in a dilution refrigerator through the superconducting transition temperature in controlled levels of magnetic fields, we isolate the flux-induced losses and quantify the added surface resistance per unit of trapped magnetic flux. Our findings indicate that magnetic flux introduces approximately 2 nΩ/mG at 10 mK and at 6 GHz in high RRR niobium. We find that the decay rate of a 6 GHz niobium cavity at 10 mK which contains a native niobium pentoxide will be dominated by the TLS oxide losses until vortices begin to impact T_1 for trapped magnetic field (B_{trap}) levels of >100 mG. In the absence of the niobium pentoxide, $B_{\text{trap}} = 10$ mG limits $Q_0 \sim 10^{10}$, or $T_1 \sim 350$ ms, highlighting the importance of magnetic shielding and magnetic hygiene in enabling $T_1 > 1$ s. We observe that the flux-induced resistance decreases with temperature-yet remains largely field-independent, qualitatively explained by thermal activation of vortices in the flux-flow regime. We present a phenomenological model which captures the salient experimental observations. Our results suggest that niobium-based transmon qubits could be robust against vortex dissipation up to several hundreds mG. We are directly addressing vortex losses in transmon qubits made with low RRR Nb films in a separate experimental study.

The widespread adoption of niobium for quantum computing applications has produced three-dimensional (3-D) superconducting radio-frequency (SRF) resonators with lifetimes T_1 up to 2 seconds of coherence [1, 2] and two-dimensional qubits with $T_1 \sim 600\mu\text{s}$ [3]. However, further improvements are necessary to realize a quantum computer capable of practical computation. This requires identifying and mitigating every loss channel present in complex multilayer, nonlinear qubit elements, including quasiparticles [4, 5], radiation [6], and two-level systems (TLS) [7]. Recent efforts have identified several such sources of decoherence in these integrated systems, including highly-lossy silicon substrates [8] and oxygen vacancies in the niobium pentoxide as a source of TLS [1, 9, 10]. On the other hand, material purity has been shown to play a lesser role in enabling high Q_0 in niobium-based resonators in the quantum regime [11], further motivating its use in quantum computing applications. These findings have aided in the development of mitigation strategies which yield substantially improved two-dimensional (2-D) transmon qubit metrics [3]. However, there remains a phenomenon of superconducting niobium which has not yet been characterized at the fields and temperatures relevant for 2-D and 3-D quantum computing architectures: trapped magnetic flux.

The effect of trapped magnetic flux under the influence

of radio-frequency (RF) fields in niobium has been widely studied in the context of particle accelerator applications [12]. Under ideal conditions, cooling a niobium cavity through the transition temperature T_c should expel incident static magnetic field via the Meissner effect. However, lattice defects and other inhomogeneities may pin flux lines and trap vortices. The vortices then interact with incident RF fields and introduce additional surface resistance via $R_s = R_T + R_0 + R_{\text{F1}}$, where R_T , R_0 , and R_{F1} are the surface resistance due to quasi-particles, material properties, and trapped magnetic flux, respectively. Moreover, it has shown that large thermal gradients supply a thermal depinning force which sweeps the vortices to regions of lower electric field and minimizes losses [13]. This finding has led to the development of cool down protocols which enable ultra-high $Q_0 > 2 \times 10^{11}$ post cooling in ambient magnetic fields of 190 mG [14]. We note, however, that such cool down protocols are not achievable in the slow and nearly homogeneous cooling provided by dilution refrigerators, indicating that any incident magnetic field is trapped in devices. To quantify these losses, previous studies have introduced the sensitivity to trapped magnetic field $S = R_{\text{F1}}/B_{\text{trap}}$, where B_{trap} is the amount of trapped magnetic field in the cavity walls [15]. Studies have shown that varying the electronic mean free path (MFP) within the penetration depth in niobium cavities results in a bell-shaped dependence of S , ranging from 0.5-1.5 nΩ/mG at 5 MV/m at a temperature of 1.5 K and frequency of 1.3 GHz [15] due to the interplay of the flux-pinning and flux-flow regimes

* dbafia@fnal.gov

[16]. This effect has not been explored in niobium at the low electric fields and milli-Kelvin temperatures relevant for quantum computing and may potentially introduce substantial degradation in complex, multi-layer qubit systems.

In this work, we directly quantify the dissipation introduced by trapped magnetic flux in niobium at millikelvin and low photon counts using a single interface, high quality factor niobium SRF cavity. By cooling a niobium SRF cavity down in controlled levels of applied magnetic fields within a dilution refrigerator, we trap various levels of magnetic vortices in the cavity walls and demonstrate a monotonic degradation in Q_0 due to an increase in flux-driven loss. We extract out the sensitivity to trapped magnetic flux and show that while it is field-independent at low fields, it decreases with increasing temperature. This is qualitatively explained by the thermal activation of vortices in the flux-flow regime which resembles two-level system behavior. At ~ 10 mK, the sensitivity is $2 \text{ n}\Omega/\text{mG}$. For a fully oxidized 6 GHz niobium cavity, trapped flux starts to contribute to limiting T_1 for $B_{\text{trap}} > 100 \text{ mG}$. In the absence of niobium pentoxide, $B_{\text{trap}} \sim 10 \text{ mG}$ will limit 3-D niobium cavities to $T_1 \sim 350 \text{ ms}$. These results suggest that trapped magnetic flux hosted in the niobium capacitor pads of transmon qubits should remain robust against vortex driven losses for large magnetic fields of several hundreds mG.

Fig. 1a) illustrates the experimental setup. We employed a 6 GHz niobium TESLA-shaped SRF cavity [17] that underwent a standard treatment process—removing $160 \mu\text{m}$ from the inner surface via buffer chemical polishing, followed by annealing at 800°C for 3 hours in ultra-high vacuum and subsequent high pressure rinsing [12]. Such treatments have been shown to yield clean cavities, with electronic MFP values of approximately 1000 nm near the inner surface [15].

As shown in Fig. 1b), the cavity was thermally anchored to the mixing chamber (MXC) plate of a dilution refrigerator and equipped with two single-axis flux gates at the equator along with a RuOx temperature sensor at the bottom flange. Helmholtz coils were mounted on either side of the cavity cell, facilitating cooling down through the transition temperature of 9.2 K in distinct magnetic field environments, thus varying the level of magnetic vortices trapped in the cavity walls. Table I presents the conditions of the four cool downs discussed here. Between each cool down, we warmed the fridge to at least 15 K and adjusted the applied magnetic field. While the near unity ratio of $B_{\text{SC}}/B_{\text{BC}}$ in Table I suggests that nearly all incident flux is trapped in the cavity walls such that $B_{\text{trap}} \approx B_{\text{NC}}$ [18], its consistency between cool downs also confirms similar thermal dynamics. Once the cavity was well below T_c , the Helmholtz coils and flux gates were powered off to minimize heat deposition. The ambient magnetic field near the cavity with the Helmholtz coils off was $-10 \pm 6.1 \text{ mG}$.

We measured cavity quality factor using methods similar to those laid out in Ref. [1]. With a vector network

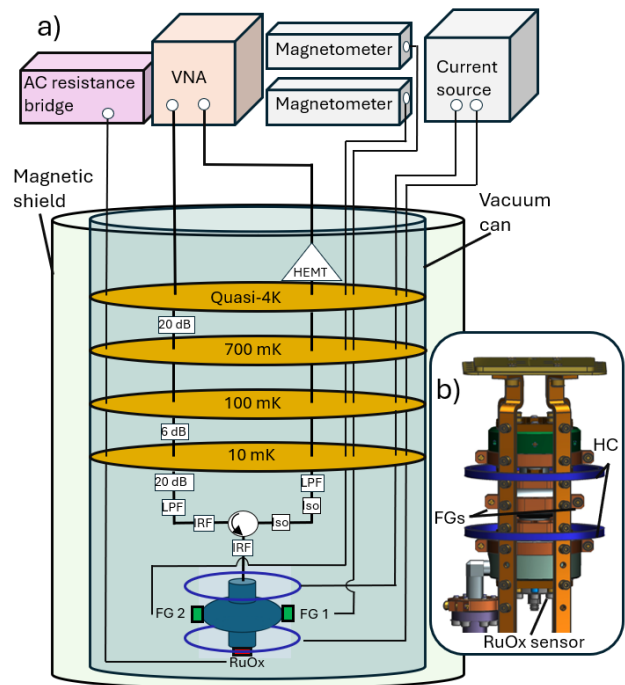


FIG. 1. a) Cartoon schematic of the setup used for our study. The measurement chain includes 46 dB of attenuation, low pass filters (LPF), infrared radiation filters (IRF), a circulator, isolators (Iso) and +35 dB HEMT amplifier. A double layer of mu-metal magnetic shielding was used to minimize the ambient magnetic field within the DR. The Helmholtz coils (HC) are shown in blue. Flux gate (FG) and RuOX temperature (RuOx) sensor positions are also presented. b) A depiction of the 6 GHz cavity with thermal anchoring and the precise location of the Helmholtz coils and diagnostic equipment.

analyzer, we first measured the resonance frequency. We then performed time-domain zero span decay measurements of the transmitted power $P_T(t)$ at this frequency after shutting off the incident signal. The first derivative of the resulting curve was used to obtain field resolved measurements of the cavity loaded quality factor Q_L . We extracted the intrinsic quality factor via $Q_0 = (1/Q_L - 1/Q_1)^{-1}$, where $Q_1 = 1.4 \times 10^9$ is the antenna quality factor obtained by circle fitting reflection scattering parameter data. We swept the DR temperature from 10 mK to 1.3 K by applying current to a heater located on the MXC plate. At each intermediate temperature, we allowed the DR to thermalize for at least two hours while acquiring decay data, verified by the RuOx temperature sensor. Thermalized data was averaged and used for our analysis. We used the amplified Johnson-Nyquist thermal noise from the HEMT amplifier to estimate the actual P_T emitted from the cavity and obtained the on-axis electric field via $E_{\text{acc}} \propto \sqrt{P_T Q_1}$.

Fig. 2 presents a subset of the data acquired from the four cool downs. In the absence of trapped magnetic flux, we observe the expected behaviors as a function of both

CD#	Current (mA)	B_{NC} (mG)	B_{SC} (mG)	B_{SC}/B_{NC}
1	3.45	0.0 ± 5.2	-0.1 ± 6.4	-
2	20.25	50.4 ± 7.5	51.3 ± 7.7	1.02
3	37.20	100.9 ± 9.0	102.5 ± 9.3	1.02
4	87.46	250.5 ± 13.3	254.8 ± 13.7	1.02

TABLE I. Flux gate readings measured for each cool down (CD) above (B_{SC}) and below ($B_{NC} \approx B_{\text{trap}}$) the niobium transition temperature along with the current applied to the Helmholtz coils. Error values capture the difference in magnetic field readings between the two flux gates due to the presence of magnetic contamination, such as the right-angle valve of the cavity.

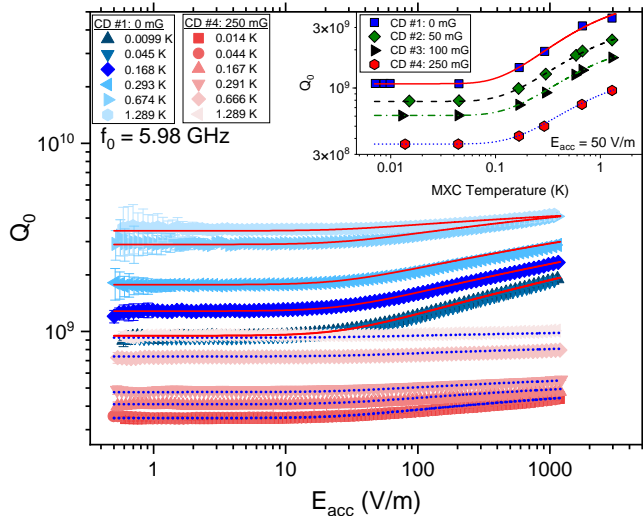


FIG. 2. Quality factor vs on-axis electric field of a 6 GHz cavity measured at temperatures ranging from 0.010 K to 1.289 K after cooling in various applied magnetic fields. Inset shows quality factor measured at an on-axis field of 50 V/m for each of the four cool downs. Blue, green, black, and red-hued points correspond to data acquired post cooling in 0 mG, 50 mG, 100 mG, and 250 mG, as described in Table I. Solid red, dashed black, dotted dashed green, and dotted blue solid lines are fits with Eq. 3; Table II presents the parameters used to model the data acquired at an electric field strength of 50 V/m. Only the data for CD #1 and CD #4 is shown in the main figure to enhance plot clarity.

temperature and field due to the gradual saturation of TLS localized in the niobium oxide [9]. As the level of trapped magnetic field in the cavity walls increases, we find an overall reduction in Q_0 .

We now extract the sensitivity to trapped magnetic flux. We isolate flux-based losses in CD #2-4 by subtracting off the contribution from material origins obtained in CD #1 and normalizing by the level of trapped field, such that

$$S = \frac{R_{\text{Fl}}}{B_{\text{trap}}} = \frac{G}{B_{\text{trap}}} \left(\frac{1}{Q_{0,n}} - \frac{1}{Q_{0,1}} \right), \quad (1)$$

where $G = 275 \Omega$ is a geometric constant and $Q_{0,n}$ and $Q_{0,1}$ is the data acquired from CD # $n = 2-4$ and CD #1,

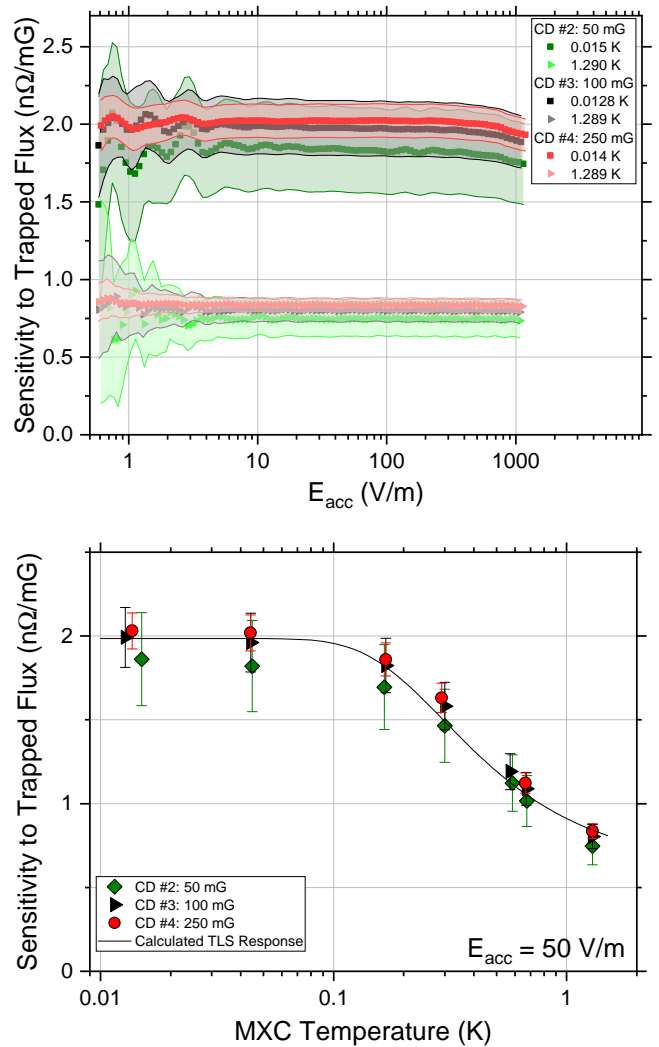


FIG. 3. Sensitivity to trapped magnetic flux as a function of a) field at temperatures of approximately 0.014 K and 1.289 K and b) temperature at 50 V/m post cooling in various magnetic fields. Color assignments are consistent with those presented in Fig. 2. Error bars represent the propagated uncertainty arising from data scatter and the applied magnetic field uncertainty. The solid black line shows a normalized TLS response, as discussed in the main text.

respectively. The results are presented in Fig. 3. Data obtained from different cool down cycles agree within the error bars, reinforcing confidence in the trapped field levels in the cavity walls and demonstrating repeatability of our measurements. In Fig. 3a), the sensitivity remains largely independent of E_{acc} below fields of 1000 V/m. To maintain plot clarity, we only present results obtained near 0.014 K and 1.289 K, as data collected at intermediate temperatures exhibit similar behavior. In contrast, Fig. 3b) reveals that S saturates below approximately 100 mK to a value of 2 nΩ/mG. As temperature increases, sensitivity decreases, following a trend reminiscent of TLS behavior.

We compare our experimental results with those of

Martinello *et al.* [15], considering differences in frequency, field, and temperature. First, Checchin *et al.* demonstrate that S is frequency independent for the MFP considered here [16]. As a result, we assume that fluxoids will respond linearly with incident RF fields such that S remains field-independent up to the MV/m range. Finally, we estimate from Fig. 3b) that $S \approx 0.78$ nΩ/mG at 1.5 K—an excellent agreement with data from similarly baked and buffer chemical polished cavities reported by Martinello.

Next, we compare our results with the calculated dissipation in type-I superconductors using the model of Andreev [19], following the derivation presented by Catelani *et al.* [20]. While the formalism is appropriate for type-I superconductors, niobium is a weak type-II superconductor and exhibits type-II/1 superconductivity in the clean limit [21, 22]. The dissipation introduced from the motion of normal regions in the flux-flow dissipation regime normalized by the amount of trapped magnetic field is given as

$$S = \frac{R_{\text{Fl}}}{B_{\text{trap}}} = \sqrt{\frac{\mu_0 \omega \rho_n}{2}} \frac{1}{B_c}, \quad (2)$$

where μ_0 , ρ_n , and B_c ($= 0.2$ T) are the vacuum permeability, normal conducting resistivity just above T_c , and thermodynamic critical field. To determine ρ_n for our niobium, we scale the room-temperature resistivity (1.5×10^{-7} Ω m) by a residual resistivity ratio of 300—typical for similarly processed niobium cavities—resulting in 5.0×10^{-10} Ω m. Substituting these values into Eq. 2 yields 1.72 nΩ/mG, which agrees with the low-temperature data presented in Fig. 3 within the error bars.

The trends observed in Figs. 2 and 3 may be qualitatively explained by assuming a linear response, thermal activation model of vortices. As discussed by Checchin [23], vortex response to RF fields in niobium cavities with a large MFP and at high frequency lies in the flux-flow regime. In this regime, Lorentz force on vortices from the incident RF fields exceeds the pinning force from defects, causing them to drift in the material. These drifting vortices respond linearly with field such that the dissipation remains field-independent. However, as the temperature increases, vortices acquire energy proportional to $k_B T$, allowing them to more easily overcome pinning potentials and experience increased viscous drag $\eta \propto 1/\rho_n$ [24]. This, in turn, reduces the energy dissipation per vortex.

We introduce a modified, phenomenological version of the standard TLS response model [1, 25] with added terms to capture quasi-particle and flux-related to model our data. The overall loss of the system is given as

$$\frac{1}{Q_0(E_{\text{acc}}, T)} = \frac{1}{Q_{\text{Ox},0}} \frac{\tanh\left(\alpha \frac{\hbar\omega}{2k_B T}\right)}{\left(1 + \left(\frac{E_{\text{acc}}}{E_c}\right)^2\right)^\gamma} + \frac{1}{Q_{\text{qp}}} + \frac{1}{Q_{\text{Fl},0}} \frac{\tanh\left(\beta \frac{\hbar\omega}{2k_B T}\right)}{\left(1 + \left(\frac{E_{\text{acc}}}{E_c}\right)^2\right)^\gamma} + \frac{1}{Q_{\text{Fl,Res}}}, \quad (3)$$

where $1/Q_{\text{Ox},0}$ and $1/Q_{\text{Fl},0}$ are the zero-temperature dielectric loss tangents associated with the niobium oxide and trapped magnetic flux, respectively, E_c is the characteristic saturation field for TLS, ω is the radial frequency, \hbar and k_B are the reduced Planck and Boltzmann constants, α , β and γ are fit parameters, and $1/Q_{\text{qp}}$ and $1/Q_{\text{Fl,Res}}$ are the quasiparticle and residual trapped flux contributions. Model parameters are presented in Table II. The fitted parameters for CD#1 are in good agreement with previously reported values [1]. Flux-driven losses show a nearly linear increase in both $1/Q_{\text{Fl},0}$ and $1/Q_{\text{Fl,Res}}$. By using the model parameters for CD #4 from Table II in the flux-dependent component of Eq. 3 and normalizing by $B_{\text{trap}} = 250$ mG, we accurately reproduce the observed trends, as demonstrated by the black solid line in Fig. 3. While this phenomenological model captures the salient features of our data, we are working toward a first-principles understanding.

	CD#1	CD#2	CD#3	CD#4
$1/Q_{\text{Ox},0}$ [$\times 10^{-10}$]	7.38	7.38	7.38	7.38
$1/Q_{\text{qp}}$ [$\times 10^{-10}$]	1.87	1.87	1.87	1.87
$1/Q_{\text{Fl},0}$ [$\times 10^{-10}$]	-	2.38	5.00	12.82
$1/Q_{\text{Fl,Res}}$ [$\times 10^{-10}$]	-	1.11	2.22	5.56

TABLE II. Parameters used to model the data in Fig. 2 using Eq. 3 at 50 V/m.

Our results suggest that trapped magnetic flux is crucial for very high Q_0 niobium cavities not dominated by other loss mechanisms such as the niobium pentoxide [1, 9]. To illustrate this, we plot $T_1 = \omega^{-1}[(1/Q_{\text{Ox},0}) + (SB_{\text{trap}}/G)]^{-1}$ for a 6 GHz niobium SRF cavity, where $Q_{\text{Ox},0}$ is the zero temperature quality factor of a fully oxidized niobium cavity; the result is plotted in Fig. 4. For $B_{\text{trap}} < 25$ mG, the native niobium oxide limits T_1 to 25 ms; trapped flux begins to impact T_1 for B_{trap} levels of >100 mG. In the absence of Nb_2O_5 , we predict that $B_{\text{trap}} = 10$ mG would yield $T_1 \sim 350$ ms, in rough agreement with the 5 GHz cavity post *in situ* oxide removal shown in Romanenko [1].

Scaling these results for a typical transmon qubit geometry [3] suggests that 500 mG would limit niobium pads to $Q_0 \sim 4 \times 10^7$. This is in agreement with previous studies, where aluminum and rhenium qubits show little additional loss post cooling in applied fields of 500 mG [26]. Instead, vortices may be used as a potential strategy for reducing the impact of quasiparticles in qubits [27]. Nevertheless, we emphasize the importance of magnetic shielding and maintaining magnetic hygiene to minimize these losses.

While the above estimates assume S for high RRR Nb, it provides an order of magnitude estimate for dirtier material. Due to the bell-shaped curve of S with mean free path [15, 23], we assume that the magnitude of loss originating from the dirty limit, flux-pinning regime is similar to that obtained in the clean limit, flux-flow regime. Intermediate values of RRR, however, will increase S , thus highlighting the importance of material properties in this

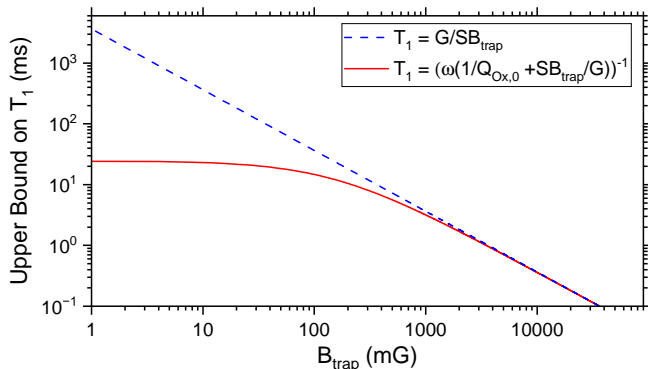


FIG. 4. Calculated upper bounds on T_1 of a niobium SRF cavity at 6 GHz considering convolved oxide and vortex contributions (solid red line) and vortex losses in the absence of oxide (blue dashed).

effect. We are directly addressing vortex losses in transmon qubits made with low RRR Nb films in a separate experimental study.

In conclusion, we have shown that trapped magnetic

vortices can drive a non-negligible level of RF loss in niobium at millikelvin and at low electric fields, relevant for 3-D resonators and 2-D devices. We find that, while these losses are field-independent, our data is accurately modeled by incorporating a thermal activation mechanism of vortices in the flux-flow regime and present a phenomenological model. At 10 mK and 6 GHz, trapped flux contributes losses of 2 n Ω /mG. Consequently, in the absence of niobium pentoxide, trapping 10 mG would limit 3-D cavity photon lifetimes to $T_1 \sim 350$ ms while having a relatively small impact on the niobium capacitor pads of transmon qubits. Our results underscore the crucial role magnetic shielding and magnetic hygiene of components in minimizing flux-related losses, required to enable quantum computing and sensing architectures with ultra-long coherence lifetimes of $T_1 > 1$ s.

We would like to thank James Sauls, Mehdi Zarea, and Andrei Lunin for insightful discussions. This material is based upon work supported by the U.S. Department of Energy, Office of Science, National Quantum Information Science Research Centers, Superconducting Quantum Materials and Systems Center (SQMS) under Contract No. DE-AC02-07CH11359.

-
- [1] A. Romanenko, R. Pilipenko, S. Zorzetti, D. Frolov, M. Awida, S. Belomestnykh, S. Posen, and A. Grassellino, Three-dimensional superconducting resonators at $T_c < 20$ mK with photon lifetimes up to $\tau = 2$ s, *Phys. Rev. Appl.* **13**, 034032 (2020).
 - [2] O. Milul, B. Guttel, U. Goldblatt, S. Hazanov, L. M. Joshi, D. Chausovsky, N. Kahn, E. Çiftiyürek, F. Lafont, and S. Rosenblum, Superconducting cavity qubit with tens of milliseconds single-photon coherence time, *PRX Quantum* **4**, 030336 (2023).
 - [3] M. Bal, A. A. Murthy, and S. Zhu et al., Systematic improvements in transmon qubit coherence enabled by niobium surface encapsulation, *npj. Quantum Inf* **10** (2024).
 - [4] P. J. de Visser, D. J. Goldie, P. Diener, S. Withington, J. J. A. Baselmans, and T. M. Klapwijk, Evidence of a nonequilibrium distribution of quasiparticles in the microwave response of a superconducting aluminum resonator, *Phys. Rev. Lett.* **112**, 047004 (2014).
 - [5] S. E. de Graaf, L. Faoro, L. B. Ioffe, S. Mahashabde, J. J. Burnett, T. Lindström, S. E. Kubatkin, A. V. Danilov, and A. Y. Tzalenchuk, Two-level systems in superconducting quantum devices due to trapped quasiparticles, *Science Advances* **6**, eabc5055 (2020).
 - [6] J. M. Martinis, Saving superconducting quantum processors from decay and correlated errors generated by gamma and cosmic rays, *Npj Quantum Inf.* **7**, 90 (2021).
 - [7] C. Müller, J. H. Cole, and J. Lisenfeld, Towards understanding two-level-systems in amorphous solids: insights from quantum circuits, *Reports on Progress in Physics* **82**, 124501 (2019).
 - [8] M. Checchin, D. Frolov, A. Lunin, A. Grassellino, and A. Romanenko, Measurement of the low-temperature loss tangent of high-resistivity silicon using a high- q superconducting resonator, *Phys. Rev. Appl.* **18**, 034013 (2022).
 - [9] D. Bafia, A. Murthy, A. Grassellino, and A. Romanenko, Oxygen vacancies in niobium pentoxide as a source of two-level system losses in superconducting niobium, *Phys. Rev. Appl.* **22**, 024035 (2024).
 - [10] P. G. Pritchard and J. M. Rondinelli, Suppressed paramagnetism in amorphous ta2o5-x oxides and its link to superconducting qubit performance, arXiv:2410.13160.
 - [11] B. Abdisatarov, D. Bafia, A. Murthy, G. Ereemeev, H. E. Elsayed-Ali, J. Lee, A. Netepenko, C. P. A. Carlos, S. Leith, G. J. Rosaz, A. Romanenko, and A. Grassellino, Direct measurement of microwave loss in Nb films for superconducting qubits, *Applied Physics Letters* **125**, 124002 (2024).
 - [12] H. Padamsee, J. Knobloch, and T. Hays, *RF Superconductivity for Accelerators* (Wiley-VCH Verlag GmbH and Co., KGaA, Weinheim, 1998).
 - [13] A. Romanenko, A. Grassellino, O. Melnychuk, and D. A. Sergatskov, Dependence of the residual surface resistance of superconducting radio frequency cavities on the cooling dynamics around T_c , *Journal of Applied Physics* **115**, 184903 (2014).
 - [14] A. Romanenko, A. Grassellino, A. C. Crawford, D. A. Sergatskov, and O. Melnychuk, Ultra-high quality factors in superconducting niobium cavities in ambient magnetic fields up to 190 mG, *Applied Physics Letters* **105**, 234103 (2014).
 - [15] M. Martinello, A. Grassellino, M. Checchin, A. Romanenko, O. Melnychuk, D. A. Sergatskov, S. Posen, and J. F. Zasadzinski, Effect of interstitial impurities on the field dependent microwave surface resistance of niobium, *Appl. Phys. Lett.* **109**, 062601 (2016).
 - [16] M. Checchin, M. Martinello, A. Grassellino, S. Aderhold, S. K. Chandrasekaran, O. S. Melnychuk, S. Posen, A. Romanenko, and D. A. Sergatskov, Frequency dependence

- of trapped flux sensitivity in srf cavities, *Applied Physics Letters* **112**, 072601 (2018).
- [17] B. Aune *et al.*, Superconducting tesla cavities, *Phys. Rev. ST Accel. Beams* **3**, 092001 (2000).
- [18] S. Posen, M. Checchin, A. C. Crawford, A. Grassellino, M. Martinello, O. S. Melnychuk, A. Romanenko, D. A. Sergatskov, and Y. Trenikhina, Efficient expulsion of magnetic flux in superconducting radiofrequency cavities for high q applications, *Journal of Applied Physics* **119**, 213903 (2016).
- [19] A. Andreev, Electrodynamics of the intermediate state, *Soviet Physics JETP* **24** (1967).
- [20] G. Catelani, K. Li, C. J. Axline, T. Brecht, L. Frunzio, R. J. Schoelkopf, and L. I. Glazman, Ac losses in field-cooled type i superconducting cavities, *Superconductor Science and Technology* **35**, 065016 (2022).
- [21] S. Ooi, M. Tachiki, T. Konomi, T. Kubo, A. Kikuchi, S. Arisawa, H. Ito, and K. Umemori, Observation of intermediate mixed state in high-purity cavity-grade nb by magneto-optical imaging, *Phys. Rev. B* **104**, 064504 (2021).
- [22] R. Prozorov, M. Zarea, and J. A. Sauls, Niobium in the clean limit: An intrinsic type-i superconductor, *Phys. Rev. B* **106**, L180505 (2022).
- [23] M. Checchin, M. Martinello, A. Grassellino, A. Romanenko, and J. F. Zasadzinski, Electron mean free path dependence of the vortex surface impedance, *Superconductor Science and Technology* **30**, 034003 (2017).
- [24] Y. B. Kim, C. F. Hempstead, and A. R. Strnad, Flux-flow resistance in type-ii superconductors, *Phys. Rev.* **139**, A1163 (1965).
- [25] D. P. Pappas, M. R. Vissers, D. S. Wisbey, J. S. Kline, and J. Gao, Two level system loss in superconducting microwave resonators, *IEEE Transactions on Applied Superconductivity* **21**, 871 (2011).
- [26] C. Song, T. W. Heitmann, M. P. DeFeo, K. Yu, R. McDermott, M. Neeley, J. M. Martinis, and B. L. T. Plourde, Microwave response of vortices in superconducting thin films of re and al, *Phys. Rev. B* **79**, 174512 (2009).
- [27] C. Wang, Y. Y. Gao, I. M. Pop, U. Vool, C. Axline, T. Brecht, R. W. Heeres, L. Frunzio, M. H. Devoret, G. Catelani, L. I. Glazman, and R. J. Schoelkopf, Measurement and control of quasiparticle dynamics in a superconducting qubit, *Nat. Comm.* **5**, 5836 (2014).